Ocean Sci. Discuss., 11, 1–35, 2015
www.ocean-sci-discuss.net/11/1/2015/
doi:10.5194/osd-11-1-2015

Ocean Science Discussions
Open Access

Typhoon effect on Kuroshio and Green Island wake: a modelling study

T.-W. Hsu[1,2], M.-H. Chou[2], T.-H. Hou[2], and S.-J. Liang[3]

[1]Research Center for Ocean Energy and Strategies, National Taiwan Ocean University, Keelung, Taiwan
[2]Department of Hydraulic and Ocean Engineering, National Cheng-Kung University, Tainan, Taiwan
[3]Department of Marine Environmental Informatics, National Taiwan Ocean University, Keelung, Taiwan

Received: 15 October 2015 – Accepted: 4 December 2015 – Published:

Correspondence to: S.-J. Liang (sjliang@ntou.edu.tw)

Published by Copernicus Publications on behalf of the European Geosciences Union.

Abstract

Green Island located in the typhoon active eastern Taiwan coastal water is the potential Kuroshio power plant site. In this study, a high resolution (250–2250 m) shallow-water equations (SWEs) model is used to investigate the effect of typhoon on the hydrodynamics of Kuroshio and Green Island wake. Two wind induced flows, typhoon Soulik and Holland's wind field model, are studied. Simulation results of the typhoon Soulik indicate that salient characteristics of Kuroshio and downstream island wake seems less affected by the typhoon Soulik because typhoon Soulik is 250 km away Green Island and the wind speed near Green Island is small. Moreover, Kuroshio currents increase when flow is in the same direction as the counterclockwise rotation of typhoon, and vice versa. This finding is in favorable agreements with the TOROS observed data.

The SWEs model, forced by the Kuroshio and Holland's wind field model, successfully reproduces the downstream recirculation and meandering vortex street. Numerical results unveil that the slow moving typhoon has a more significant impact on the Kuroshio and downstream Green Island wake than the fast moving typhoon does. Due to the counterclockwise rotation of typhoon, Kuroshio currents increase (decrease) in the right (left) of the moving typhoon's track. This rightward bias phenomenon is evident, especially when typhoon moves in the same direction as the Kuroshio mainstream.

1 Introduction

According to Zdravkovich (2003) flow past a bluff obstacle with the Reynolds number $Re = u_\infty L / \nu_t$ in the range of 50 and 800, a well-organized downstream wake occurs, where u_∞ is the characteristic flow velocity, L the characteristic length, and ν_t the eddy viscosity of fluid. Flow becomes periodic with detachment of the free shear layer, and consequently alternate shedding of vortices. The periodic phenomenon is referred to as the vortex shedding, where the anti-symmetric clockwise and counterclockwise wake pattern is called as to the von Karman vortex streets (Zdravkovich, 2003).

Vortex streets occur frequently in the atmosphere and oceans (Chelton et al., 2011; Nunalee and Basu, 2014). The phenomenon of vortex shedding behind bluff bodies has long been of interest to the fluid dynamics community and has been intensively studied by many researchers (Zdravkovich, 2003; Roshko, 2012; Tritton, 1959; Williamson, 1996). The downstream island wakes produce the upwelling and enhance the nitrate concentration in the upper ocean. This kind of phenomenon is often captured by satellite imagery (Hubert and Krueger, 1962; Li et al., 2000; Thomson et al., 1977; Young and Zawislak, 2006; Zheng et al., 2008), field measurement (Barkley, 1972), and by numerical modeling (Dong et al., 2007; Heywood et al., 1996; Ruscher and Deardorff, 1982; Wolanski et al., 1984).

The Kuroshio, a western boundary current of the sub-tropic North Pacific Ocean, originates from the North Equatorial Current and flows northward to the eastern coast of Taiwan. The passage of the Kuroshio mainstream parallels to the eastern shoreline of Taiwan. Green Island is located at (121°28′ E, 22°35′ N) and is 40 km off the southeastern coast of Taiwan. The climatology of the Kuroshio velocity as revealed from in situ measurements shows that Green Island is approximately located in the mainstream of the energetic Kuroshio passage and acts as an obstacle to the stream. Hence downstream island wakes are prone to occur. Characteristics of the vortex streets downstream Green Island can be found from the MODIS (moderate resolution imaging spectroradiometer) satellite images and in situ measurements (Chang et al., 2013). Seasonal variation of mainstream, current patterns, and transport of the Kuroshio in the east of Taiwan has been numerically investigated (Hsin et al., 2008). Spatial and temporal scales of downstream Green Island wake due to passing of the Kuroshio has been numerically studied (Liang et al., 2013). The seasonal wind-, heat flux-, and buoyancy-driven circulation and thermohaline structure of the Caspian Sea is numerically investigated (Gunduz and Özsoy, 2014). Salient features of the mesoscale dynamics, mixing and transport of the Caspian Sea is well reproduced, and compared well with the observation.

Typhoons, also known as tropical low-pressure cyclones, occur in the tropical and subtropical seas, and are a frequent cause of serious disasters in coastal countries and regions. Taiwan is located in the Northwest Pacific – one of the most typhoon active areas of the world. An annual average of four to five typhoons hit the island according to the records of the Central Weather Bureau (CWB) of Taiwan (http://www.cwb.gov.tw/) over the past century (1958–2009). Typhoons typically occur in the period from late April to December, but with most storms concentrated in July through September. In recent years, the number of typhoons and the maximum wind speed increase, and the center pressure of typhoons decreases due to the climate change.

Typhoons have a significant impact on the physical and chemical characteristics of the water of the Kuroshio. The storms disturb the Kuroshio's path and reduce its flow rate, while strengthens upwelling and lowering the surface temperature. The impact of typhoons on the upper water layers is quite dramatic in the Kuroshio. Suda (1943) suggested that typhoons are the main cause for the Kuroshio meandering near Japan. Sun et al. (2008) conducted a numerical analysis for the impact of typhoons on the Kuroshio's path south of Japan, found that violent disturbances on the sea surface caused by a typhoon produces a strong upwelling, further strengthens the counter-clockwise eddy and causes the Kuroshio to deviate southward from original path by about 2° of latitude. Chen et al. (2013) suggested that, in the sea as east Taiwan, typhoons with a diameter exceeding 200 km (a large counterclockwise eddy) can reduce significantly the Kuroshio's flow volume and cause a 180° change of the Kuroshio flow direction.

Taiwan has an excellent marine current energy resource as it is an island country and experiences the abundant marine current flows. However, this resource has yet to be explored. The Kuroshio is known for its strong and fast flow. It could be a potential source of renewable energy as it flow steadily all year round, and Green Island is the potential test site for Kuroshio current energy of Taiwan. Chen (2013) proposed

Title Page
Abstract | Introduction
Conclusions | References
Tables | Figures
◂ | ▸
Back | Close
Full Screen / Esc
Printer-friendly Version
Interactive Discussion

a conceptual design for the Kuroshio power plant. Assessment of potential Kuroshio power test site has been performed using the in situ measurements and modelling by Hsu et al. (2015). Safety, maintenaces and operations of the Kuroshio power plant may be subject to impacts from earthquakes, typhoons, climate change, and other natural factors. To prevent the potential damages caused by typhoon-driven waves, meandering vortex shedding, and the cavitation occurred on the surface of turbine blade, turbines and platforms should be submerged several tens of meters below the water surface. Effect of monsoon on the Green Island wake has been previously studied (Hsu et al., 2015; Liu et al., 1992). The effect of typhoon on the Kuroshio and Green Island wake is presented using a high resolution (250–2250 m) SWEs model in this study.

2 Theory and numerical method

Shallow-water equations (SWEs) for describing the shallow water flows and space-time least-squares finite-element method (STLSFEM) used to solve SWEs are briefly introduced in this section.

2.1 Shallow-Water Equations

The two-dimensional vertical-averaged SWEs are a simple form for describing the horizontal structure of the ocean dynamics (Buachart et al., 2014; Johnson, 1997; Tan, 1992; Vreugdenhil, 2013). The two-dimensional viscous SWEs in a non-conservative form read

$$\frac{\partial \eta}{\partial t} + \frac{\partial}{\partial x}[(H+\eta)u] + \frac{\partial}{\partial y}[(H+\eta)v] = 0 \tag{1}$$

$$\frac{\partial u}{\partial t} + u\frac{\partial u}{\partial x} + v\frac{\partial u}{\partial y} + g\frac{\partial \eta}{\partial x} - fv = -g\frac{\partial Z_\mathrm{b}}{\partial x} + \frac{\tau_x^\mathrm{s}}{\rho h} + \frac{\rho \nu_t}{h}\left[2\frac{\partial(hu)}{\partial x} + \left(\frac{\partial(hv)}{\partial x} + \frac{\partial(\rho u)}{\partial y}\right)\right]$$

$$\frac{\partial v}{\partial t} + u\frac{\partial v}{\partial x} + v\frac{\partial v}{\partial y} + g\frac{\partial \eta}{\partial y} + fu = -g\frac{\partial Z_\mathrm{b}}{\partial y} + \frac{\tau_y^\mathrm{s}}{\rho h} + \frac{\rho \nu_t}{h}\left[\left(\frac{\partial (hv)}{\partial x} + \frac{\partial (\rho u)}{\partial y}\right) + 2\frac{\partial (hv)}{\partial y}\right]$$

where η is the water surface elevation, t is time, H is the still water depth, $h = H + \eta$ is the total water depht, u is the x component velocity, v is the y component velocity, Z_b is the bottom height, and ν_t is the eddy viscosity which is an important parameter for modeling the Reynolds stresses for the fluid (Yulistiyanto et al., 1998). τ_x^b and τ_y^b representing the x and y component bottom frictional shear stresses are expressed as

$$\tau_x^\mathrm{b} = \rho C_{D_\mathrm{b}} \sqrt{u^2 + v^2}\, u \tag{2}$$

$$\tau_y^\mathrm{b} = \rho C_{D_\mathrm{b}} \sqrt{u^2 + v^2}\, v \tag{3}$$

where C_{D_b} is the coefficient of bottom friction ranging between 0.0025 to 0.0040 for ocean modeling (Martin and McCutcheon, 1998).

Holland's wind field model (Holland et al., 2010) is employed to compute the typhoon wind field. The equation of the gradient of wind speed is

$$W_\mathrm{g} = \left[\frac{100\,B\,(p_n - p_\mathrm{c})\left(R_\mathrm{mw}/r\right)^B}{\rho_\mathrm{air} e^{\left(R_\mathrm{mw}/r\right)^B}}\right]^{\frac{1}{2}} \tag{4}$$

where B is a scaling number, p_n is the ambient pressure, p_c is the pressure of typhoon center, R_mw is the radius of maximum wind speed, r is the radius to typhoon center, and $\rho_\mathrm{air} = 1.2\,\mathrm{kg\,m^{-3}}$ is the air density.

The wind shear stresses on the water surface are usually expressed in terms of the wind speed at 10 m above the water surface W_{10}. Powell (1980) suggested that the relationship between the gradient of wind speed W_g and W_{10} can be expressed as $W_{10} = 0.8\,W_\mathrm{g}$. Therefore, τ_x^s and τ_y^s representing the x and y component wind shear

OSD
11, 1–35, 2015

stresses are given as

$$\tau_x^{\mathrm{s}} = \rho_{\mathrm{air}} C_{D_{\mathrm{s}}} \sqrt{W_{10x}^2 + W_{10y}^2}\, W_{10x} \tag{5}$$

$$\tau_y^{\mathrm{s}} = \rho_{\mathrm{air}} C_{D_{\mathrm{s}}} \sqrt{W_{10x}^2 + W_{10y}^2}\, W_{10y} \tag{6}$$

Where W_{10x} and W_{10y} are the x and y component of W_{10}, $C_{D_{\mathrm{s}}}$ is the coefficient of surface stresses (Zhang and Sannasiraj, 2008).

2.2 Space–Time Least-Squares Finite-Element Method

We use the two-dimensional SWEs to illustrate the Space–Time Least-Squares Finite-Element Method (STLSFEM). The two-dimension SWEs read

$$\begin{aligned}
&\frac{\partial \eta}{\partial t} + u\frac{\partial (H+\eta)}{\partial x} + (H+\eta)\frac{\partial u}{\partial x} + v\frac{\partial (H+\eta)}{\partial y} + (H+\eta)\frac{\partial v}{\partial y} = 0\\
&\frac{\partial u}{\partial t} + u\frac{\partial u}{\partial x} + v\frac{\partial u}{\partial y} = S_x\\
&\frac{\partial v}{\partial t} + u\frac{\partial v}{\partial x} + v\frac{\partial v}{\partial y} = S_y
\end{aligned} \tag{7}$$

where $S_x = \frac{\tau_x^{\mathrm{s}} - \tau_x^{\mathrm{b}}}{\rho h} - g\frac{\partial Z_{\mathrm{b}}}{\partial x}$, $S_y = \frac{\tau_y^{\mathrm{s}} - \tau_y^{\mathrm{b}}}{\rho h} - g\frac{\partial Z_{\mathrm{b}}}{\partial y}$. The Newton method is applied to linearize the nonlinear terms in Eq. (7), and the resulting equations are

$$\begin{aligned}
&\frac{\partial \eta}{\partial t} + H\frac{\partial u}{\partial x} + u\frac{\partial H}{\partial x} + \frac{\partial}{\partial x}\left(\tilde{\eta}u + \eta\tilde{u} - \tilde{\eta}\tilde{u}\right) + H\frac{\partial v}{\partial y} + v\frac{\partial H}{\partial y} + \frac{\partial}{\partial y}\left(\tilde{\eta}v + \eta\tilde{v} - \tilde{\eta}\tilde{v}\right) = 0\\
&\frac{\partial u}{\partial t} + \left(\tilde{u}\frac{\partial u}{\partial x} + u\frac{\partial \tilde{u}}{\partial x} - \tilde{u}\frac{\partial \tilde{u}}{\partial x}\right) + \left(\tilde{v}\frac{\partial u}{\partial y} + v\frac{\partial \tilde{u}}{\partial y} - \tilde{v}\frac{\partial \tilde{u}}{\partial y}\right) = \tilde{S}_x\\
&\frac{\partial v}{\partial t} + \left(\tilde{u}\frac{\partial v}{\partial x} + u\frac{\partial \tilde{v}}{\partial x} - \tilde{u}\frac{\partial \tilde{v}}{\partial x}\right) + \left(\tilde{v}\frac{\partial v}{\partial y} + v\frac{\partial \tilde{v}}{\partial y} - \tilde{v}\frac{\partial \tilde{v}}{\partial y}\right) = \tilde{S}_y
\end{aligned} \tag{8}$$

OSD
11, 1–35, 2015

where the symbol "∼" denotes the value from the previous iteration or time step. In the STLSFEM, the unknowns $\underset{\sim}{u} = \{\eta, u, v\}^T$ are approximated by the polynomial interpolations

$$\begin{Bmatrix} \eta(x,y,t) \\ u(x,y,t) \\ v(x,y,t) \end{Bmatrix} = \begin{bmatrix} M(x,y)N(t) \\ M(x,y)N(t) \\ M(x,y)N(t) \end{bmatrix} \begin{Bmatrix} \eta \\ u \\ v \end{Bmatrix} \tag{9}$$

where $M(x)$ and $N(t)$ are the space and time interpolation functions, respectively. Substituting the approximations Eq. (9) into Eq. (10), the residuals can be written as

$$\begin{Bmatrix} R^e_\eta \\ R^e_u \\ R^e_v \end{Bmatrix} = \begin{bmatrix} MN_2' & (HM_x + H_xM)N_2 & \left(HM_y + H_yM\right)N_2 \\ 0 & MN_2' + \{\tilde{u}M_x + \tilde{u}_xM + \tilde{v}M_y\}N_2 & \tilde{u}_yMN_2 \\ 0 & \tilde{v}_xMN_2 & MN_2' + \{\tilde{u}M_x + \tilde{v}M_y + \tilde{v}_yM\}N_2 \end{bmatrix} \begin{Bmatrix} \eta \\ u \\ v \end{Bmatrix}^{n+1} + \begin{bmatrix} MN_1' & (HM_x + H_xM)N_1 & \left(HM_y + H_yM\right)N_1 \\ 0 & MN_1' + \{\tilde{u}M_x + \tilde{u}_xM + \tilde{v}M_y\}N_1 & \tilde{u}_yMN_1 \\ 0 & \tilde{v}_xMN_1 & MN_1' + \{\tilde{u}M_x + \tilde{v}M_y + \tilde{v}_yM\}N_1 \end{bmatrix} \begin{Bmatrix} \eta \\ u \\ v \end{Bmatrix}^{n} + \begin{Bmatrix} \tilde{S}_\eta \\ \tilde{S}_u \\ \tilde{S}_v \end{Bmatrix} \tag{10}$$

Note that a piecewise continuous linear interpolation function for time is used, where the subscripts 1 and 2 denote the number of spatial local nodes, and superscripts n and $n+1$ denote the values of the space-time element at $t = t^n$ and $t = t^{n+1}$, respectively.

Upon applying the least square method, we thus have

$$\min \int_{\Omega_{xt}} R^2 d\Omega \tag{11}$$

where $R = \left\{R^e_\eta, R^e_u, R^e_v\right\}^T$ are the residuals, Ω_{xt} are the element of the space-time. Equation (11) can be rewritten in the form

$$\int_{\Omega_{xt}} \left\{\frac{\partial R}{\partial \underset{\sim}{u}}\right\} R d\Omega = 0 \tag{12}$$

Details of the STLSFEM can be found in Gunzburger (2012), Hughes and Hulbert (1988), Jiang (2013), Laible and Pinder (1993), Liang and Hsu (2009).

3 Computed results and discussions

In this section, the effect of typhoon Soulik and wind field of Holland's model (Holland et al., 2010) on the Kuroshio and Green Island wake are presented.

3.1 Typhoon Soulik

A high resolution (250–2250 m) SWEs model is used to investigate the hydrodynamic characteristics of the Kuroshio and downstream Green Island wake. Green Island locates at (121°28′ E, 22°350′ N), 40 km off the southeastern coast of Taiwan. Figure 1a depicts the study domain, location of Lanyu Island and Green Island, and bathymetry of the adjacent sea waters. The bathymetry of the study area varies from 400 to 5000 m, with an average value about 2000 m. The bathymetry around the Green Island is within the range from 500 to 4000 m, with an average value of 2000 m. There

OSD
11, 1–35, 2015

are sea-mountains in the northwest of the Green Island where water depth varying from 200 to 400 m.

However, Kuroshio is a sub-surface flow where flow mainly occurs at the top 400 m layer of water with an average current speed around 1.0 $\mathrm{m\,s^{-1}}$; Water below 800 m is essentially motionless (Chang et al., 2013). Therefore, we limit the bathymetry ranging from 10 to 360 m as the redefined bathymetry from the ETOPO1 in the simulations. Figure 1b depicts the computational meshes. It contains 50 842 nodes and 101 125 triangles. Spatial resolution varies from 250 to 2250 m. Fine meshes are employed near Lanyu Island and Green Island since flow field is expected to change dramatically in these areas.

The flow field data of HYCOM (HYbrid Coordinate Ocean Model) on 7 November 2014 after interpolation to the model grids, shown in Fig. 2a, is utilized to initiate the model. The choice of this particular flow field as the initial condition is based on the hypothesis proposed by Zheng and Zheng (2014) in which the downstream Green Island wake is prone to occur when Kuroshio mainstream heads on the island. Figure 2b shows the boundaries of the study domain. $\overline{AB}$ is the land boundary where no flux and free-slip boundary condition is applied, $\overline{BC}$ is the open boundary where the radiation boundary conditions is specified, and $\overline{CD}$, $\overline{DO}$, and $\overline{OA}$ are the velocity boundaries using the flow field data from HYCOM on 7 November 2014.

Figure 3 shows a composite ERS-1 SAR image of downstream island vortex trains of Lanyu Island and Green Island taken with one week interval sequentially between 17:01 UT 25 September (lower) and 19:02 UT 2 October (top), 1996. Two downstream island vortex trains are clearly seen. One a little far from the coast, called the Lanyu Island (also called the Orchid Island) vortex train, occurs downstream of Lanyu Island (a little beyond the southern boundary of image), and consists of three vortexes, two cyclonic appearing as bright shading and one anticyclonic appearing as dark shading vortexes. Another near the eastern coast of Taiwan, called the Green Island vortex train, occurs downstream of Green Island, and consists of three pairs of cyclonic vortexes (bright center) and anticyclonic vortexes (dark center). Spatial and temporal

OSD
11, 1–35, 2015

scales of downstream Green Island wake due to passing of the Kuroshio has been numerically studied (Liang et al., 2013). The main difference between Liang et al. (2013) and the present study lies in the point that a constant inflow used in Liang et al. (2013) is replaced by a spatial varying inflow from HYCOM in the present study.

The SWEs model is applied to simulation the typhoon Soulik event. Typhoon Soulik hit Taiwan area during 7 to 14 July 2013. Figure 4 depicts the track of typhoon Soulik. Typhoon Soulik, developed from a tropic depression on 7 July 2013 through a tropical storm, moderate typhoon, severe typhoon, and then to decrease its strength and make landfall on Taiwan on 7 December 2013. The typhoon Soulik data with the temporal interval every 6 h are from the CWB of Taiwan, which are computed by the NFS (Non-hydrostatic Forecast System). NFS uses the structured orthogonal meshes, however, SWEs model uses the unstructured triangular meshes. Therefore, wind data needs to be interpolated into the computational nodes of the SWEs model. The IDW (inverse distance weighted interpolation; Shepard, 1962) is employed to interpolate the data from NFS into nodal points of the SWEs model. In this study, the 5 km resolution typhoon Soulik data is used. The maximum wind speed of typhoon Soulik is 51 m s^{-1}, categorized as a severe typhoon. The closest distance of typhoon to Green Island is about 250 km. The maximum wind speed of the model area is 17 m s^{-1} and the average value is smaller than 10 m s^{-1}.

Figure 5a depicts the global view of the study area, where the enclosed region near the Green Island indicates the sub-domain that will be presented in the succeeding plots of the downstream recirculation and island wakes. Figure 5b depicts the local view of the sub-domain as well as location of the cross section $\overline{Q_0Q_1}$ and monitor point P downstream Green Island, where time series of flow quantities are presented and analyzed. Length of $\overline{Q_0Q_1}$ is 20 km. It locates about 22 km downstream the Green Island.

Figure 6 depicts the typhoon wind field and flow streamlines as well as vectors of wind (red) and flow (blue) along cross section $\overline{Q_0Q_1}$ at S_0–S_4 five time instances with a 12 h of increment, shown in Fig. 5, where S_0 represents 00:00 of 12 July, S_1 12:00

of 12 July, S_2 00:00 of 13 July, S_3 12:00 of 13 July, and S_4 00:00 of 14 July, 2013, respectively. As can be seen, the downstream island wake is well reproduced. The flow field is affected by the typhoon, especially in the shallow water area and the lee of the islands. Interactions of Kuroshio and downstream island wake with typhoon is obvious. When typhoon approaches the study area, because of the cyclonic rotation and southward winding of typhoon, Kuroshio current decreases. At S_3, it is the moment when the center of typhoon is closest to the Green Island. The wind starts to change its direction and to blow northward. Comparing flow vectors along cross section $\overline{Q_0Q_1}$ at S_2 with that at S_1 and S_3 of Fig. 6, it is noticed that downstream island wake is significantly affected. Kuroshio currents increase after S_2 due to the northward winding and resumes its normal flow condition after typhoon passes far away.

Figure 7a illustrates the location of 22.84° N (y = 150 km) cross section, where black dots denote the position of TOROS data, and Fig. 7b and c depicts the comparison of the TOROS observed surface currents with the computed flow vectors along the 22.84° N cross section at S_0–S_4 five time instances. Since TOROS data are the surface flow quantities, they are larger than the depth-averaged model predictions, in general. Moreover, the left one-third of the cross section (0–20 km) is right in the lee of Green Island. The meandering downstream island wake is observed in the modelling, but not present in the TOROS data, because of its coarse spatial resolution (~ 10 km). However, computed results show Kuroshio currents increase when flow is in the same direction as the counterclockwise rotation of typhoon, and vice versa. This finding is consistent with the TOROS measured datasets (Lu et al., 2014).

3.2 Effect of model typhoon on Green Island wake

Figure 8 depicts flow streamlines around the Green Island of no wind forcing in a period of vortex shedding. There are small recirculations in the lee of Green Island. Its size is about the size of the island (~ 8 km). of the island (~ 8 km). A well-organized coherent and alternating asymmetric meandering eddies in the lee of the Green Island is reproduced, which has been observed in field measurement (Chang et al., 2013) and satellite images (Liang et al., 2013; Zheng and Zheng, 2014). In this study, simulation using the boundary conditions based on HYCOM produces a more realistic Kuroshio flow and downstream Green Island wakes.

According to the statistical analysis of typhoons from 1911 to 2010 by the CWB of Taiwan, 83.6 % of typhoons pass the eastern Taiwan coastal waters and 13.5 % pass the western Taiwan coastal waters. Therefore, two typical tracks of typhoons, namely the SN typhoon (17 % of total) moving from southwest to northeast and the EW typhoon (67 % of total) moving from east to west, shown in Fig. 9, are chosen to investigate the effect of typhoon on the Kuroshio and Green Island wake. Two typical values of the typhoon moving speed, $2.5\,\mathrm{m\,s^{-1}}$ ($9\,\mathrm{km\,h^{-1}}$) and $5.0\,\mathrm{m\,s^{-1}}$ ($18\,\mathrm{km\,h^{-1}}$), are considered. Value of the radius of maximum wind speed $R_{\mathrm{mw}} = 50\,\mathrm{km}$ and pressure of typhoon center $p_{\mathrm{c}} = 950\,\mathrm{hPa}$ are used in the Holland's wind field model. The resulting maximum of W_{10} is about $47\,\mathrm{m\,s^{-1}}$.

In order to better quantify the net influence of typhoon on Green Island wake, we subtract the flow field of SN typhoon case and EW typhoon case with no wind forcing case. The net influence of typhoon on the flow field is defined by

$$u_{\mathrm{net}} = u_{\mathrm{wind}} - u_{\mathrm{no\ wind}} \tag{13}$$

$$v_{\mathrm{net}} = v_{\mathrm{wind}} - v_{\mathrm{no\ wind}} \tag{14}$$

Figures 10 and 11 show the "net" u and v contours of SN typhoon at T_0–T_2 three time instances as indicated in Fig. 16. It is noted that the effect of typhoon on the y component velocity are more pronounced than on the x component velocity, because the direction of moving SN typhoon and the mainstream of Kuroshio is the same, in general. Due to the counterclockwise rotation of typhoon, flow accelerates (decelerates) when it flows in the favorable (adverse) direction of wind. For example, Figs. 14 and 15 show that y component velocity increases in the right of SN typhoon's track and decreases in the left of SN typhoon's track, the so called rightward bias phenomenon. The rightward bias phenomenon of u contours is not as evident as v contours, since the

OSD
11, 1–35, 2015

northeastward Kuroshio and x component wind forcing are not in the same or opposite direction.

Comparing Fig. 10 with Fig. 11, we notice that the impact of the slow moving typhoon ($W_T = 2.5\,\mathrm{m\,s^{-1}}$) is more significant than the fast moving typhoon ($W_T = 5.0\,\mathrm{m\,s^{-1}}$), especially in the y component velocity when typhoon moves in favor of the Kuroshio mainstream direction. When typhoon moves slowly, it takes longer time to travel the same distance. Therefore, more momentum and energy are input to water, and water takes more time to respond to the wind forcing.

Figure 12 plots the wind field as well as wind vectors (red) and flow (blue) vectors along $\overline{Q_0Q_1}$ at T_0–T_2 three time instances. The flow field and downstream island wake are significantly affected by the northeastward typhoon. Kuroshio currents increase as typhoon approaches and decrease as typhoon passes away.

Figures 13 and 14 plot the "net" u and v contours of EW typhoon at T_0–T_2 three time instances indicated in Fig. 16. The rightward bias feature due to the counterclockwise rotation of typhoon is evident, especially for the slow moving typhoon and y component velocities. Comparing Figs. 10 and 11 with Figs. 13 and 14, the impact of SN typhoon on the Kuroshio and downstream Green Island wake is apparently more significant than EW typhoon. The effect of typhoon strengthens when typhoon moves in favor of the Kuroshio and weakens when typhoon moves against the Kuroshio.

Figure 15 plots the wind field as well as wind vectors (red) and flow vectors (blue) along $\overline{Q_0Q_1}$ at T_0–T_2 three time instances of EW typhoon case. The flow field and downstream island wake are also significantly affected by the EW typhoon. Kuroshio currents decrease as typhoon approaches and increase in a short period as typhoon passes away.

Figure 16 shows a comparison of time series of u and v of the monitor point P of no wind forcing case and SN typhoon case with (a) $W_T = 2.5\,\mathrm{m\,s^{-1}}$ and (b) $W_T = 5.0\,\mathrm{m\,s^{-1}}$, respectively. Three vertical lines are drawn and represent the three time instances. The first time instance (T_0), represented by the red vertical dashed line, indicates the time instance when typhoon is located 50 km southwest of Green Island. The second time instance (T_1), represented by the green vertical dashed line, indicates the moment when typhoon passes the Green Island. The third time instance (T_2), represented by the blue vertical dashed line, indicates the time instance when typhoon is located 50 km northeast of Green Island. It shows that typhoon has little influence on the flow field near P when it approaches P and is far away from P. However, the influence of typhoon increases as typhoon approaching P, and remains significant in a short period after the typhoon has passed far away P.

4 Conclusions

Safety, maintenances, and operations of Kuroshio power plant may be subject to impacts from earthquakes, typhoons, climate change, and other natural factors. Typhoons have a significant impact on the physical and chemical characteristics of the water of the Kuroshio. A shallow water model based on the shallow water equations (SWEs) and the space-time least-squares finite-element method (STLSFEM) has been developed. The model has been applied to study the hydrodynamics of Kuroshio and Green Island wakes with a small computational domain (72 km × 156 km) and coarse mesh resolution (500–3500 m; Liang et al., 2013; Hsu et al., 2015). The spatial and temporal scales of downstream Green Island wakes has been quanified and compared with the in-situ measurements and satellite images. Special efforts of the present study are made to refine the model including to integrate Holland's wind field model (Holland et al., 2010), to use a larger computational domain (124 km × 220 km) with a finer mesh resolution (250–2250 m), and to use flow field from HYCOM as the initial and boundary conditions to drive the flows.

A high resolution (250–2250 m) shallow-water model is used to investigate effect of typhoon on the hydrodynamics of the Kuroshio and Green Island wake. In the first simulation case, we simulate the typhoon Soulik event to validate the applicability of the SWEs model. Computed results indicate that salient characteristics of Kuroshio and downstream island wake seem less affected by the typhoon because typhoon is

250 km away Green Island and wind speed is smaller than $10\,\mathrm{m\,s^{-1}}$ near the region of Green Island. However, Kuroshio currents increase when flow is in the same direction as the counterclockwise rotation of typhoon, and vice versa. This finding is consistent with the TOROS observed dataset (Lu et al., 2014).

In the second simulation case, the SWEs model, forced by the Kuroshio and Holland's wind field model, successfully reproduces the downstream recirculation and meandering vortex streets. Kuroshio and the downstream Green Island wake is found significantly affected by the moving typhoon that passes the Green Island directly, especially for the shallow waters and the lee of the islands. Computed results clearly reveal the rightward bias phenomenon – due to counterclockwise rotation of typhoon, Kuroshio currents increase in the right of the moving typhoon's track and decrease in the left of the moving typhoon's track. Computed results also show that the slower the moving typhoon, the more significant impact of typhoon on the Kuroshio and downstream Green Island wake.

Acknowledgements. This study is supported by the NSC NEP-I project under the grants of NSC103-3113-P-019-001 and NSC103-3113-P-019-012.

References

Barkley, R. A.: Johnston atolls wake, J. Mar. Res., 30, 201–216, 1972.

Buachart, C., Kanok-Nukulchai, W., Ortega, E., and Onate, E.: A shallow water model by finite point method, Int. J. Comput. Meth., 11, 1350047-1–1350047-27, doi:10.1142/S0219876213500473, 2014.

Chang, M. H., Tang, T. Y., Ho, C. R., and Chao, S. Y.: Kuroshioinduced wake in the lee of Green Island off Taiwan, J. Geophys. Res.-Oceans, 118, 1508–1519, 2013.

Chelton, D. B., Schlax, M. G., and Samelson, R. M.: Global observations of nonlinear mesoscale eddies, Prog. Oceanogr., 91, 167–216, 2011.

Chen, C.-T. A., Liu, C.-T., Chuang, W., Yang, Y., Shiah, F.-K., Tang, T., and Chung, S.: Enhanced buoyancy and hence upwelling of subsurface Kuroshio waters after a typhoon in the southern East China Sea, J. Marine Syst., 42, 65–79, 2003.

Chen, F.: The Kuroshio Power Plant, The Kuroshio Power Plant, Springer, Singapore, Springer, 2013.
Dong, C., McWilliams, J. C., and Shchepetkin, A. F.: Island wakes in deep water, J. Phys. Oceanogr., 37, 962–981, 2007.
Gunduz, M. and Özsoy, E.: Modelling seasonal circulation and thermohaline structure of the Caspian Sea, Ocean Sci., 10, 459–471, doi:10.5194/os-10-459-2014, 2014.
Gunzburger, M. D.: Finite Element Methods for Viscous Incompressible Flows: a Guide to Theory, Practice, and Algorithms, Elsevier, Singapore, 2012.
Heywood, K. J., Stevens, D. P., and Bigg, G. R.: Eddy formation behind the tropical island of Aldabra, Deep-Sea Res. Pt. I, 43, 555–578, 1996.
Holland, G. J., Belanger, J. I., and Fritz, A.: A revised model for radial profiles of hurricane winds, Mon. Weather Rev., 138, 4393–4401, 2010.
Hsin, Y. C., Wu, C. R., and Shaw, P. T.: Spatial and temporal variations of the Kuroshio east of Taiwan, 1982–2005: a numerical study, J. Geophys. Res.-Oceans, 113, C04002-1–C04002-15, doi:10.1029/2007JC004485, 2008.
Hsu, T.-W., Doong, D.-J., Hsieh, K.-J., and Liang, S.-J.: Numerical study of Monsoon effect on Green Island Wake, J. Coastal Res., 31, 1141–1150, doi:10.2112/JCOASTRES-D-14-00206.1, 2015.
Hubert, L. and Krueger, A.: Satellite pictures of mesoscale eddies, Mon. Weather Rev., 90, 457–463, 1962.
Hughes, T. J. and Hulbert, G. M.: Space-time finite element methods for elastodynamics: formulations and error estimates, Comput. Method. Appl. M., 66, 339–363, 1988.
Jiang, B.-N.: The Least-Squares Finite Element Method: Theory and Applications in Computational Fluid Dynamics and Electromagnetics, Springer Science & Business Media, Berlin, German, 2013.
Johnson, R.: A Modern Introduction to the Mathematical Theory of Water Waves, Cambridge University Press, Cambridge, 1997.
Laible, J. P. and Pinder, G. F.: Solution of the shallow water equations by least squares collocation, Water Resour. Res., 29, 445–455, 1993.
Li, X., Clemente-Colón, P., Pichel, W. G., and Vachon, P. W.: Atmospheric vortex streets on a RADARSAT SAR image, Geophys. Res. Lett., 27, 1655–1658, 2000.
Liang, S.-J., and Hsu, T.-W.: Least-squares finite-element method for shallow-water equations with source terms, Acta Mech. Sinica, 25, 597–610, 2009.

Liang, S.-J., Lin, C.-Y., Hsu, T.-W., Ho, C.-R., and Chang, M.-H.: Numerical study of vortex characteristics near Green Island, Taiwan, J. Coastal Res., 29, 1436–1444, 2013.
Liu, K. K., Gong, G. C., Shyu, C. Z., Pai, S. C., Wei, C. L., and Chao, S. Y.: Response of Kuroshio upwelling to the onset of the northeast monsoon in the sea north of Taiwan: observations and a numerical simulation, J. Geophys. Res.-Oceans, 97, 12511–12526, 1992.
Lu, Y.-C., Liau, J.-M., Ou, S.-H., Lai, J.-W., Chou, M.-H., and Hsu, T.-W.: Effects of typhoon on Kuroshio current field, in: 7th Chinese-German Joint Symposium on Hydraulic and Ocean Engineering, Leibniz Universitat Hannover, Germany, September 8–12, 2014.
Martin, J. L. and McCutcheon, S. C.: Hydrodynamics and Transport for Water Quality Modeling, CRC Press, Boca Raton, 1998.
Nunalee, C. G. and Basu, S.: On the periodicity of atmospheric von Kármán vortex streets, Environ. Fluid Mech., 14, 1335–1355, 2014.
Powell, M. D.: Evaluations of diagnostic marine boundary-layer models applied to hurricanes, Mon. Weather Rev., 108, 757–766, 1980.
Roshko, A.: On the wake and drag of bluff bodies, J. Aeronaut. Sci., 22, 124–132, 2012.
Ruscher, P. H. and Deardorff, J. W.: A numerical simulation of an atmospheric vortex street, Tellus A, 34, 555–566, 1982.
Shepard, D.: A two-dimensional interpolation function for irregularly-spaced data, in: Proceedings of the 1968 23rd ACM national conference, ACM, 517–524, New York, August 27–29, 1968.
Suda, K.: The Science of the Sea (Kaiyo-Kagaku), Kokin-shoin, Tokyo, 1943.
Sun, L., Yang, Y.-J., and Fu, Y.-F.: Impacts of typhoons on the Kuroshio large meander: observation evidences, arXiv preprint, 2, 45–50, 2008.
Tan, W.-Y.: Shallow Water Hydrodynamics: Mathematical Theory and Numerical Solution for a two-dimensional System of Shallow-Water Equations, Elsevier, Singapore, 1992.
Thomson, R. E., Gower, J. F., and Bowker, N. W.: Vortex streets in the wake of the Aleutian Islands, Mon. Weather Rev., 105, 873–884, 1977.
Tritton, D. J.: Experiments on the flow past a circular cylinder at low Reynolds numbers, J. Fluid Mech., 6, 547–567, 1959.
Vreugdenhil, C. B.: Numerical Methods for Shallow-Water Flow, Springer Science & Business Media, Singapore, 2013.
Williamson, C. H.: Vortex dynamics in the cylinder wake, Annu. Rev. Fluid Mech., 28, 477–539, 1996.

OSD
11, 1–35, 2015

Wolanski, E., Imberger, J., and Heron, M.: Island wakes in shallow coastal waters, J. Geophys. Res.-Oceans, 89, 10553–10569, 1984.
Young, G. S. and Zawislak, J.: An observational study of vortex spacing in island wake vortex streets, Mon. Weather Rev., 134, 2285–2294, 2006.
Yulistiyanto, B., Zech, Y., and Graf, W.: Flow around a cylinder: shallow-water modeling with diffusion-dispersion, J. Hydraul. Eng.-ASCE, 124, 419–429, 1998.
Zdravkovich, M. M.: Flow around Circular Cylinders, Volume 2: Applications, Oxford University Press, Oxford, UK, 2003.
Zhang, H. and Sannasiraj, S.: Wind wave effects on surface stress in hydrodynamic modeling, in: The Eighth ISOPE Pacific/Asia Offshore Mechanics Symposium, International Society of Offshore and Polar Engineers, Vancouver, Canada, November 10–14, 2008.
Zheng, Q., Lin, H., Meng, J., Hu, X., Song, Y. T., Zhang, Y., and Li, C.: Submesoscale ocean vortex trains in the Luzon Strait, J. Geophys. Res.-Oceans, 113, C04032-1–C04032-12, doi:10.1029/2007JC004362, 2008.
Zheng, Z.-W. and Zheng, Q.: Variability of island-induced ocean vortex trains, in the Kuroshio region southeast of Taiwan Island, Cont. Shelf Res., 81, 1–6, 2014.

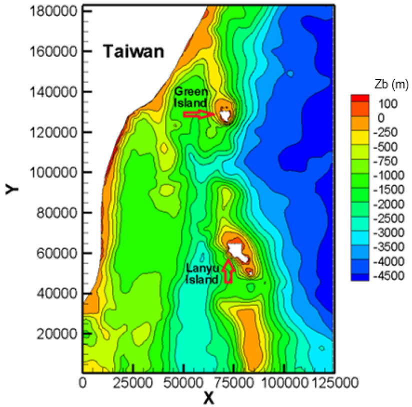

(a)

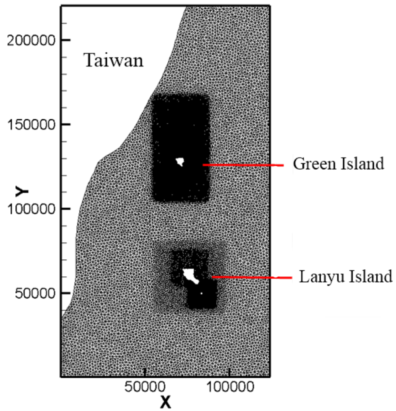

(b)

Figure 1. (a) Schematic illustration of the study domain and the bathymetry derived from the ETOPO1 and **(b)** computational meshes with fine meshes used in the coastal waters around Lanyu Island and Green Island.

OSD
11, 1–35, 2015

Typhoon effect on Kuroshio and Green Island wake: a modelling study

T.-W. Hsu et al.

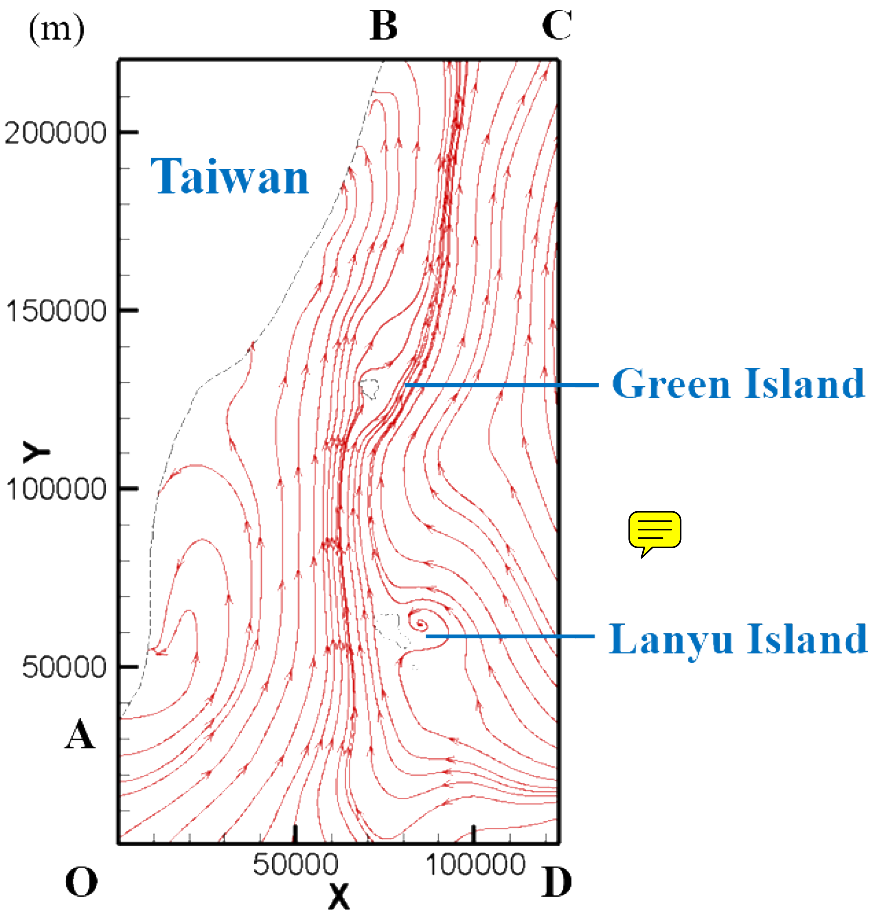

Figure 2. Study domain and boundaries as well as contours of flow speed from HYCOM.

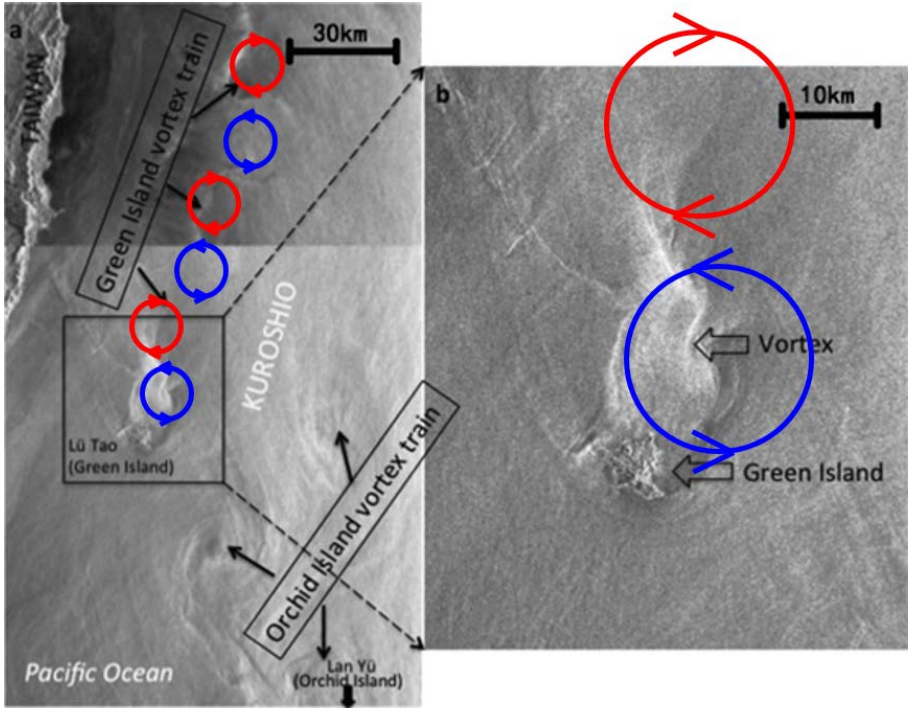

(a) (b)

Figure 3. (a) A composite ERS-1 SAR image of island-induced ocean vortex trains of Lanyu Island and Green Island taken at 17:01 UT 25 September (lower) and 19:02 UT 2 October (top), 1996. **(b)** Zoomed Green Island and head of vortex train (modified from Fig. 2 of Zheng and Zheng, 2014).

OSD
11, 1–35, 2015

Typhoon effect on Kuroshio and Green Island wake: a modelling study

T.-W. Hsu et al.

OSD
11, 1–35, 2015

Typhoon effect on Kuroshio and Green Island wake: a modelling study

T.-W. Hsu et al.

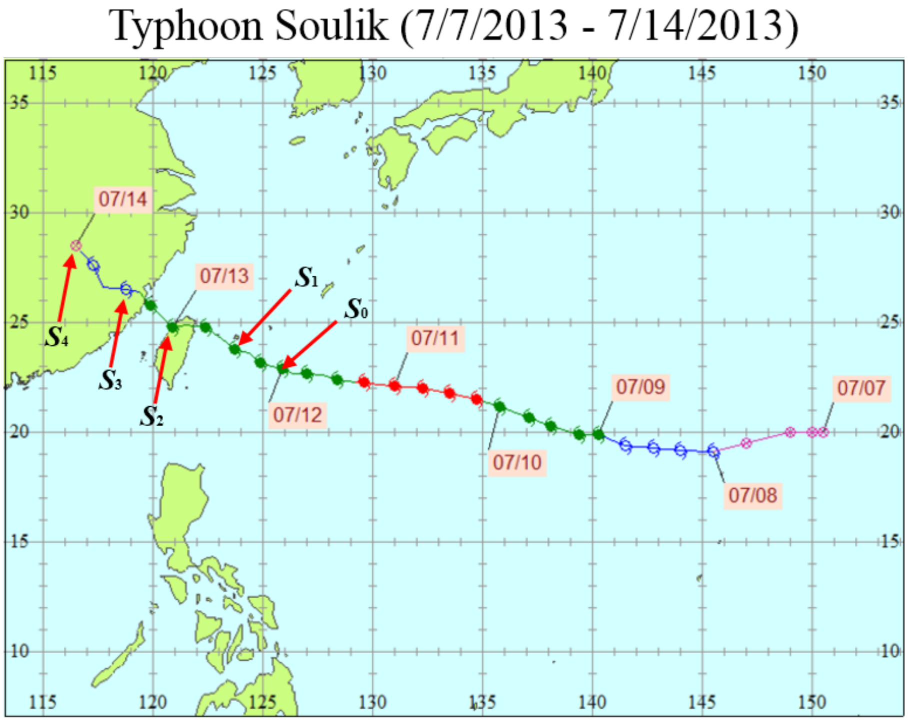

Figure 4. Track of typhoon Soulik from 7 to 14 July 2013, where symbol ⊗ denotes the tropical depression with maximum wind speed $V_{max} < 17.2\,\mathrm{m\,s^{-1}}$; the tropical storm, $17.2 < V_{max} < 32.6\,\mathrm{m\,s^{-1}}$; the moderate typhoon, $32.7 < V_{max} < 50.9\,\mathrm{m\,s^{-1}}$; a severe typhoon, $51\,\mathrm{m\,s^{-1}} < V_{max}$, and S_0–S_4 are the five time instances with a 12 h of increment to show the flow fields, see, for example, S_0 represents 00:00 of 12 July, S_1 12:00 of 12 July, S_2 00:00 of 13 July, S_3 12:00 of 13 July, and S_4 00:00 of 14 July 2013, respectively (modified from CWB of Taiwan).

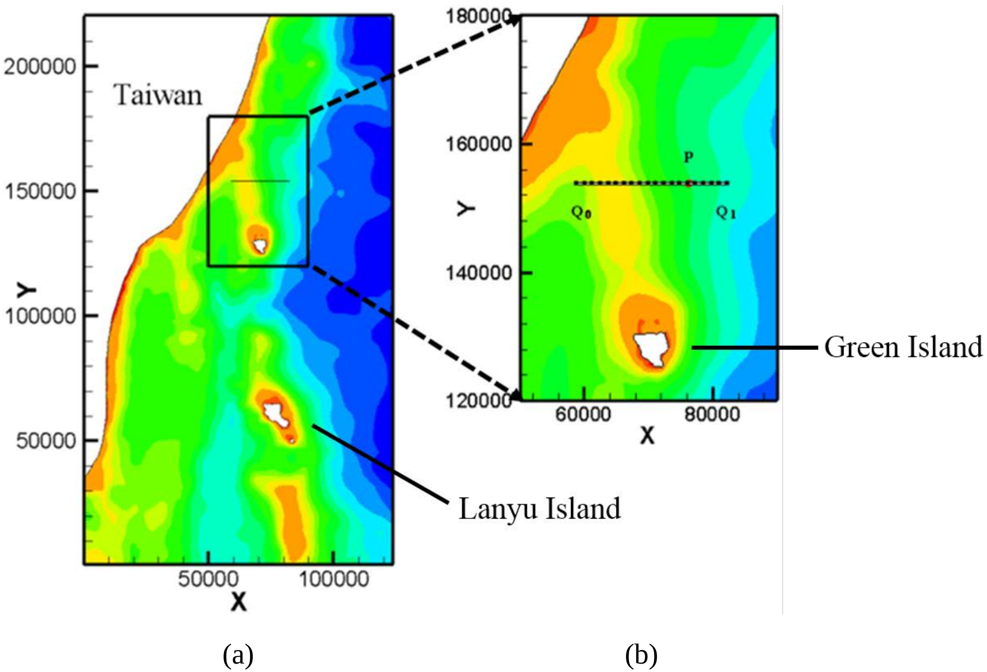

Figure 5. (a) Global view of the study area, where the enclosed region near the Green Island indicates the sub-domain that will be presented in the succeeding plots of the downstream recirculation and island wakes, and **(b)** local view of the sub-domain as well as location of the cross section $\overline{Q_0Q_1}$ and monitor point P downstream Green Island. Length of $\overline{Q_0Q_1}$ is 20 km. It locates about 22 km downstream the Green Island.

OSD
11, 1–35, 2015

Typhoon effect on Kuroshio and Green Island wake: a modelling study

T.-W. Hsu et al.

Title Page
Abstract Introduction
Conclusions References
Tables Figures
Back Close
Full Screen / Esc
Printer-friendly Version
Interactive Discussion

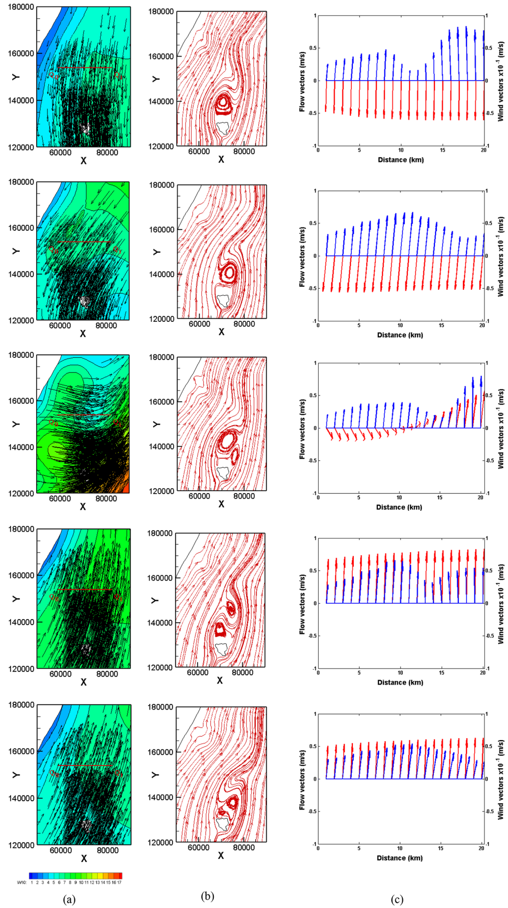

Figure 6. (a) W_{10} vectors and contours, **(b)** flow streamlines, and **(c)** wind vectors (red) and flow vectors (blue) of cross section $\overline{Q_0Q_1}$ at S_0–S_4 five time instances of the typhoon Soulik, see Fig. 5.

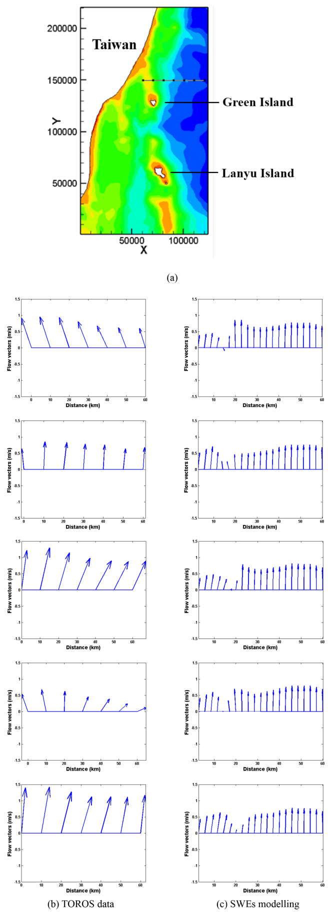

Figure 7. (a) Location of the 22.84° N (y = 150 km) cross section, where black dots denote the position of TOROS data. **(b)** and **(c)** depict comparison of flow vectors of TOROS data and model predictions along 22.84° N cross section at S_0–S_4 five time instances, see Fig. 5.

OSD
11, 1–35, 2015

Discussion Paper | Discussion Paper | Discussion Paper | Discussion Paper |

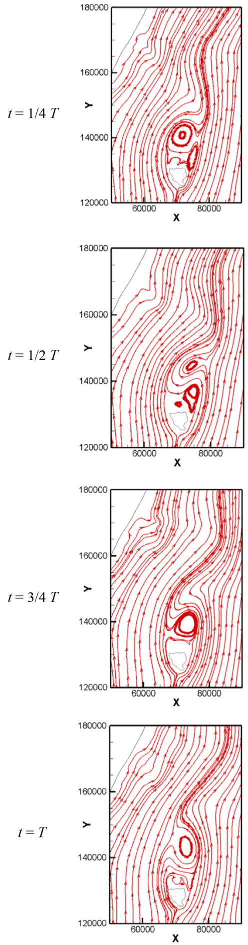

Figure 8. Flow streamlines of the Green Island wake of no wind forcing case.

OSD
11, 1–35, 2015

Typhoon effect on Kuroshio and Green Island wake: a modelling study

T.-W. Hsu et al.

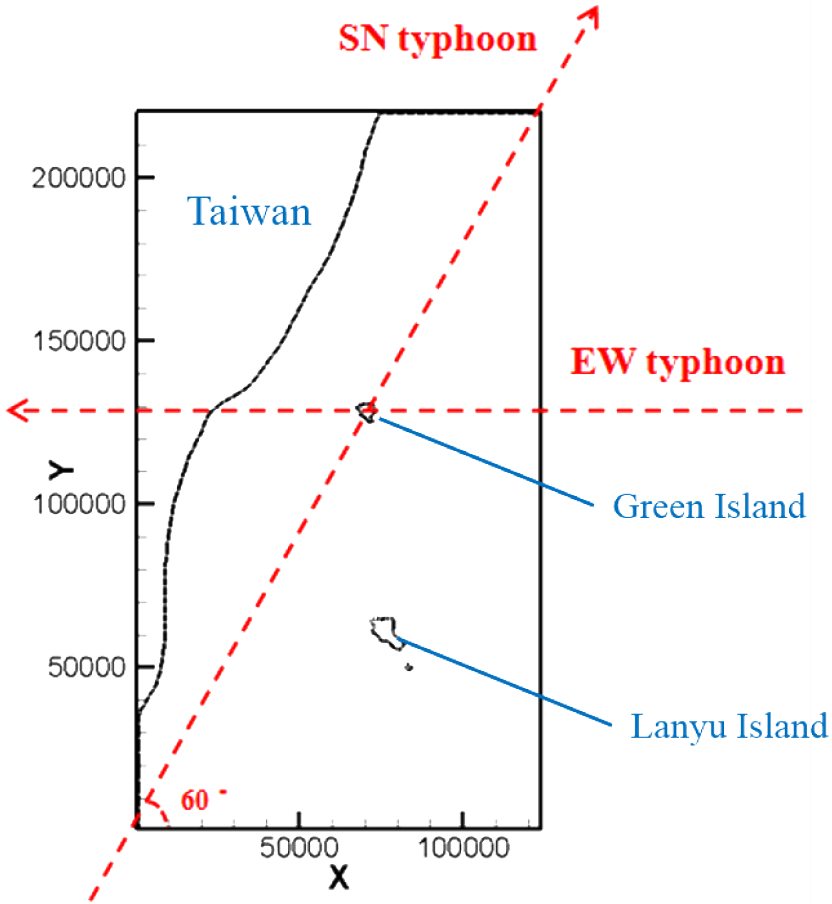

Figure 9. Schematic diagram of the study domain and track of SN and EW typhoon.

OSD
11, 1–35, 2015

Typhoon effect on Kuroshio and Green Island wake: a modelling study

T.-W. Hsu et al.

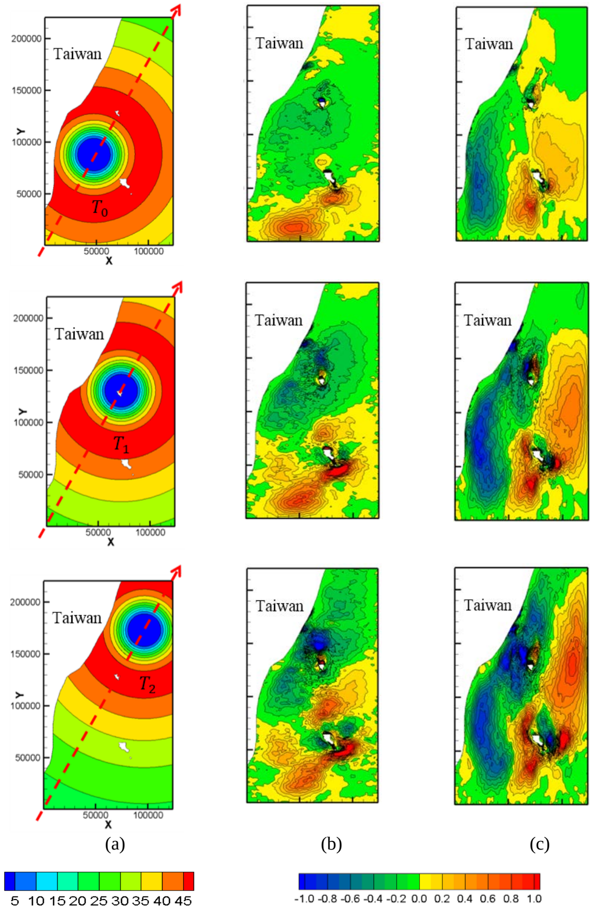

Figure 10. Contours of **(a)** W_{10}, "net" **(b)** u, and **(c)** v contours of SN typhoon with moving speed $W_T = 2.5\,\mathrm{m\,s^{-1}}$ at T_0–T_2 three time instances indicated by the three vertical lines of Fig. 16a.

OSD
11, 1–35, 2015

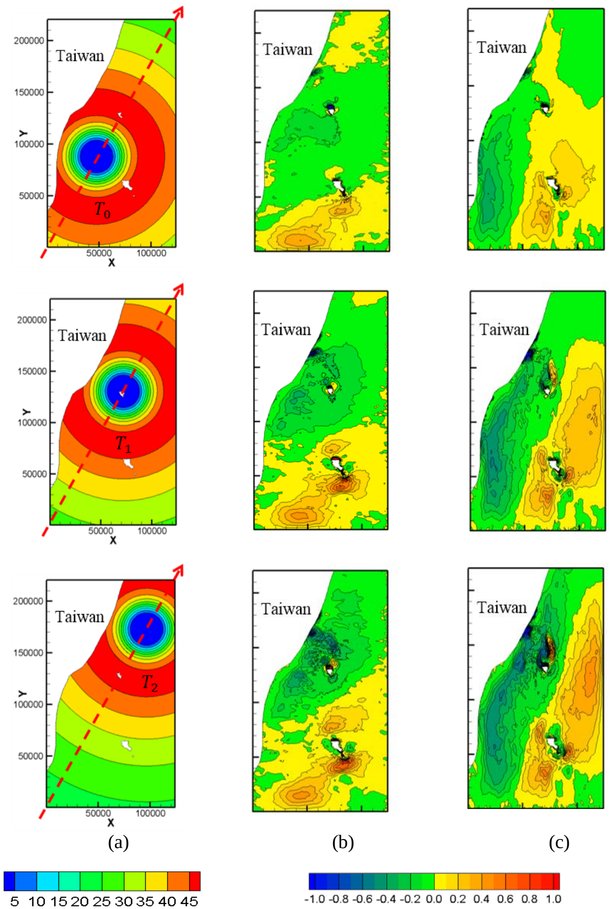

Figure 11. Contours of **(a)** W_{10}, "net" **(b)** u, and **(c)** v contours of SN typhoon with moving speed $W_T = 5.0\,\mathrm{m\,s^{-1}}$ at T_0–T_2 three time instances indicated by the three vertical lines of Fig. 16b.

OSD
11, 1–35, 2015

Typhoon effect on Kuroshio and Green Island wake: a modelling study

T.-W. Hsu et al.

Title Page
Abstract Introduction
Conclusions References
Tables Figures
Back Close
Full Screen / Esc
Printer-friendly Version
Interactive Discussion

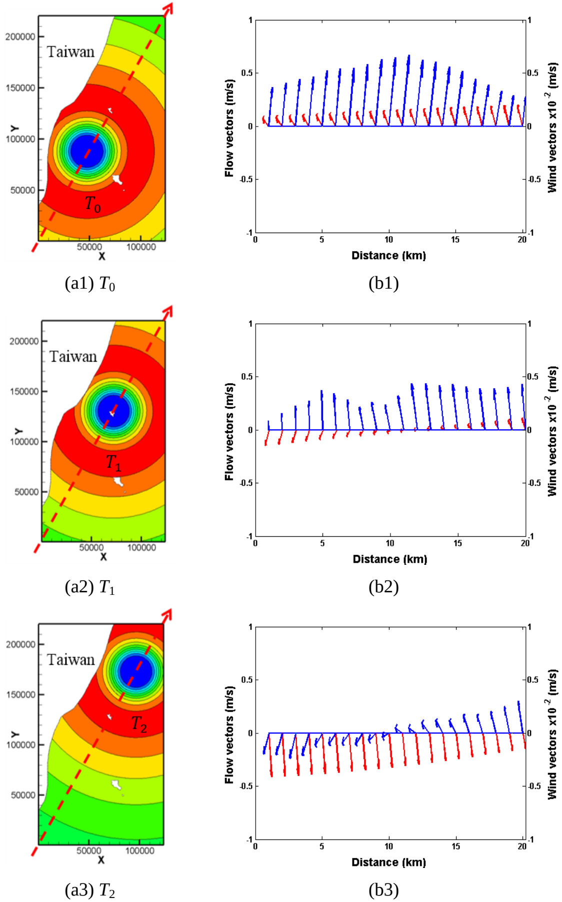

Figure 12. (a) W_{10} contours and **(b)** wind vectors (red) and flow vectors (blue) of SN typhoon along cross section $\overline{Q_0Q_1}$ with moving speed $W_T = 2.5\,\mathrm{m\,s^{-1}}$ at T_0–T_2 three time instances indicated by the three vertical lines of Fig. 16a.

OSD

11, 1–35, 2015

Typhoon effect on Kuroshio and Green Island wake: a modelling study

T.-W. Hsu et al.

Title Page
Abstract | Introduction
Conclusions | References
Tables | Figures
◄ | ►
Back | Close
Full Screen / Esc
Printer-friendly Version
Interactive Discussion

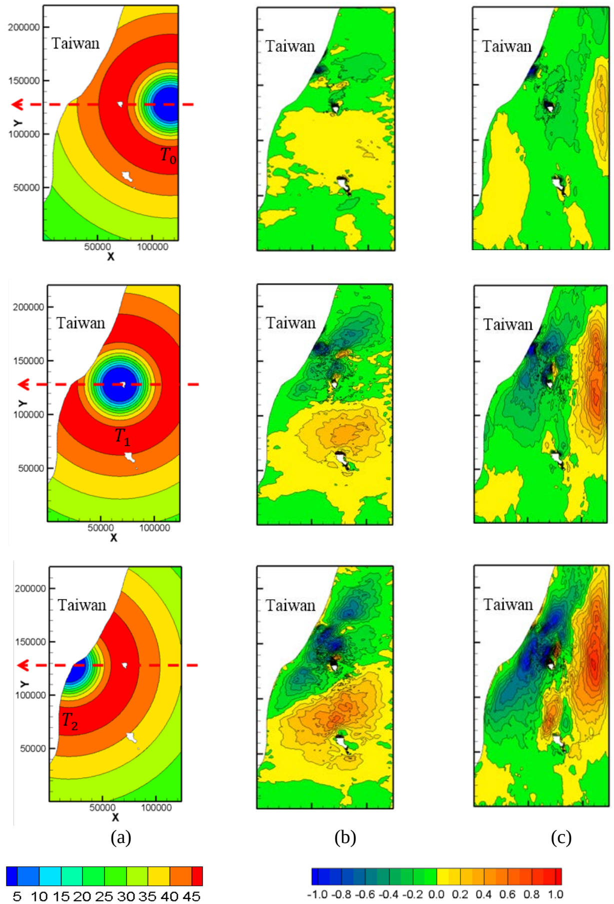

Figure 13. Contours of **(a)** W_{10}, "net" **(b)** u, and **(c)** v contours of EW typhoon with moving speed $W_T = 2.5\,\mathrm{m\,s^{-1}}$ at three time instances T_0–T_2 indicated by the three vertical lines of Fig. 16a.

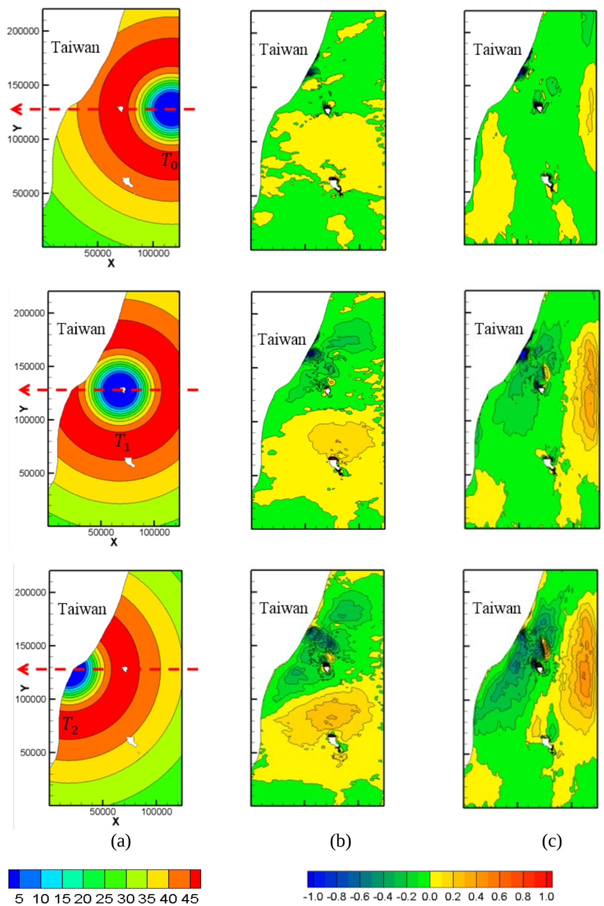

Figure 14. Contours of **(a)** W_{10}, "net" **(b)** u, and **(c)** v contours of EW typhoon with moving speed $W_T = 5.0\,\mathrm{m\,s^{-1}}$ at T_0–T_2 three time instances indicated by the three vertical lines of Fig. 16b.

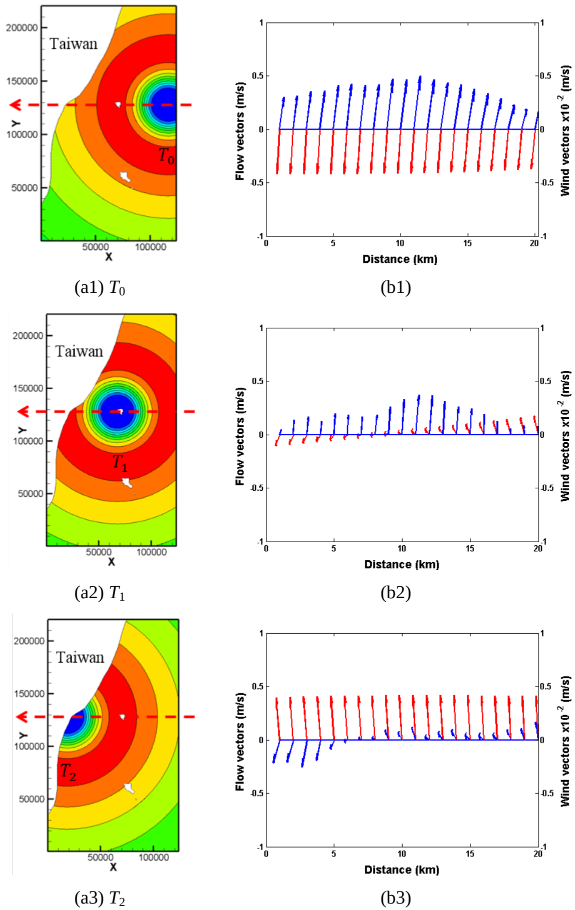

Figure 15. (a) W_{10} contours and **(b)** wind vectors (red) and flow vectors (blue) of EW typhoon along cross section $\overline{Q_0Q_1}$ with moving speed $W_T = 2.5\,\mathrm{m\,s^{-1}}$ at T_0–T_2 three time instances indicated by the three vertical lines of Fig. 16a.

OSD
11, 1–35, 2015

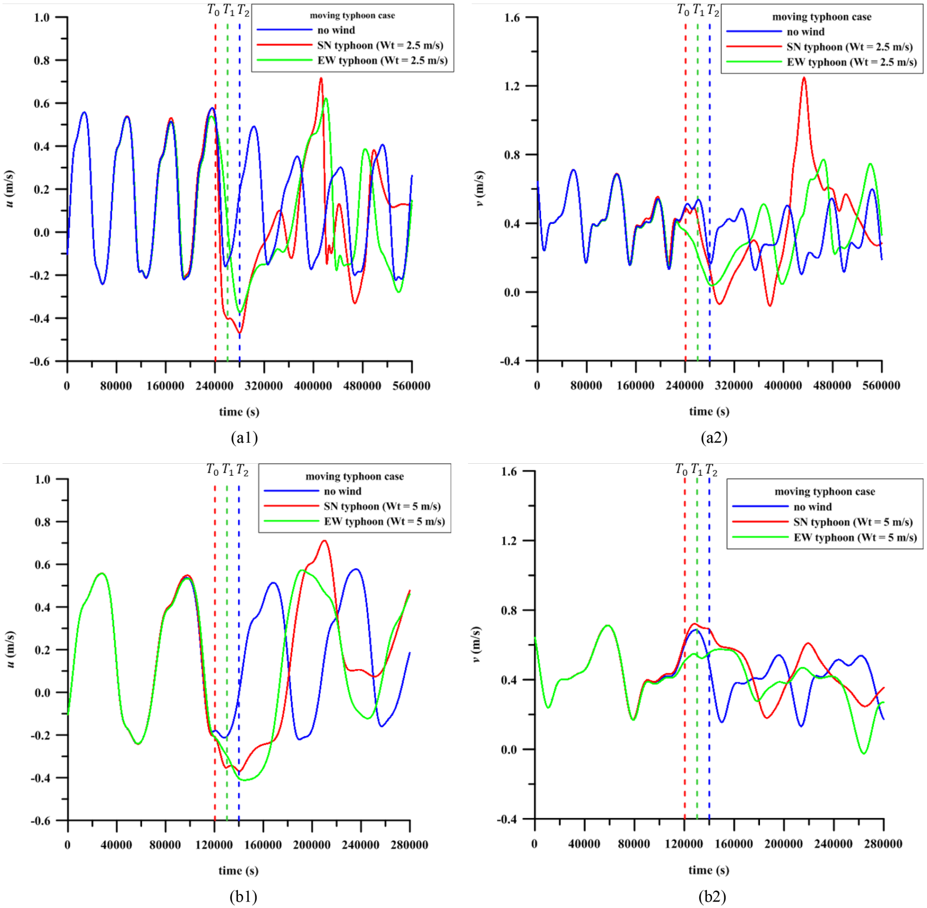

Figure 16. Comparison of u and v of monitor point P of no wind, SN, and EW typhoon with the moving speed W_T = **(a)** 2.5 m s^{-1} (upper row) and **(b)** 5.0 m s^{-1} (lower row), respectively.